Dual modality sensor using liposome-based signal amplification technique for ultrasensitive norovirus detection

Dual modality sensor using liposome-based signal amplification technique for ultrasensitive norovirus detection

Akhilesh Babu Ganganboina,[1] Ankan Dutta Chowdhury[1], Indra Memdi Khoris[2], Fahmida Nasrin[2], Kenshin Takemura[2], Toshimi Hara[3], Fuyuki Abe[3], Tetsuro Suzuki[4], Enoch Y. Park[1,2,*]

[1] Research Institute of Green Science and Technology, Shizuoka University, 836 Ohya Suruga-ku, Shizuoka 422-8529, Japan

[2] Department of Bioscience, Graduate School of Science and Technology, Shizuoka University, 836 Ohya Suruga-ku, Shizuoka 422-8529, Japan

[3] Department of Microbiology, Shizuoka Institute of Environment and Hygiene, 4-27-2, Kita-ando, Aoi-ku, Shizuoka 420-8637, Japan

[4] Department of Infectious Diseases, Hamamatsu University School of Medicine, 1-20-1 Higashi-ku, Handa-yama, Hamamatsu 431-3192, Japan

E-mail addresses:
akhilesh.babu.ganganboina@shizuoka.ac.jp (ABG)
ankan.dutta.chowdhury@shizuoka.ac.jp (ADC)
Indra.memdi.khoris.17@shizuoka.ac.jp (IMK)
fahmida.nasrin.17@shizuoka.ac.jp (FN)
takemura.kenshin.16@shizuoka.ac.jp (KT)
toshimi1_hara@pref.shizuoka.lg.jp (TH)
fuyuki1_abe@pref.shizuoka.lg.jp (FA)
tesuzuki@hama-med.ac.jp (TS)
park.enoch@shizuoka.ac.jp (EYP)

[*] Corresponding author at: Research Institute of Green Science and Technology, Shizuoka University, 836 Ohya, Suruga-ku, Shizuoka 422-8529, Japan.
E-mail address: park.enoch@shizuoka.ac.jp (E.Y. Park). Tel (Fax): +81-54-238-4887)

Abstract

Sensitive and accurate detection methods for infectious viruses are the pressing need for effective disease diagnosis and treatment. Herein, based on V_2O_5 nanoparticles-encapsulated liposomes (VONP-LPs) we demonstrate a dual-modality sensing platform for ultrasensitive detection of the virus. The sensing performance relies on intrinsic peroxidase and electrochemical redox property of V_2O_5 nanoparticles (V_2O_5 NPs). The target-specific antibody-conjugated VONP-LPs and magnetic nanoparticles (MNPs) enrich the virus by magnetic separation and the separated VONP-LPs bound viruses are hydrolyzed to release the encapsulated V_2O_5 NPs. These released nanoparticles from captured liposomes act as peroxidase mimics and electrochemical redox indicator resulting in noticeable colorimetric and robust electrochemical dual-signal. Utilizing the superiority of dual-modality sensor with two quantitative analysis forms, norovirus like particles (NoV-LPs) can be detected by electrochemical signals with a wide linear range and low detection limit. To verify the applicability in real samples, norovirus (NoV) collected from actual clinical samples are effectively-identified with excellent accuracy. This proposed detection method can be a promising next-generation bioassay platform for early-stage diagnosis of virus disease and surveillance for public health.

Keywords: Dual-modality, Norovirus, colorimetric, electrochemical, V_2O_5 nanoparticles, liposomes

1. Introduction

Viral disease outbreaks with speedy mutation and high stability within the environment result in higher mortality every year and bring huge economic losses worldwide.(Weerathunge et al., 2019; Ye et al., 2017) Besides, modern-day travel has enabled these disease agents to spread infections worldwide with high prevalence and mortality rates.(Bui et al., 2015; Zang et al., 2019) According to WHO's assessment, number of deaths in 2015, because of HEV infection is 44,000, and humans infected with influenza virus (H7N9) a total of 304 cases (including 36 deaths) from January to February of 2017.(Maurya et al., 2020) Nearly 200,000 deaths annually worldwide including 70,000 or more among children from developing countries is estimated to result because of NoV infection.(Hall et al., 2016) Therefore, fast and early detection technologies for disease biomarkers are essential to prevent disease and for advancement of standard of living, majorly for resource limited nations.

Various approaches for virus detection, such as a localized surface plasmon resonance,(Nasrin et al., 2018; Takemura et al., 2017; Wu et al., 2018) electrochemical sensors,(Anusha et al., 2019; Faria and Zucolotto 2019) and paper based analytical equipment(Bhardwaj et al., 2019) are reported recently. In pursuit of supreme performance, latest studies are emphasizing on preparing a nanomaterial for constraining increased amount of analytes for high specificity.(Chowdhury et al., 2019) However, saturation has been obtained in these methods.(Chowdhury et al. 2019) Single signal amplification methods often suffer from low sensitivity, selectivity and linearity that are unsatisfactory owing to the inadequate target specimen and diminishing of signal because of similar biomolecules. Therefore, benefits of one method could be merged with the benefits of another, simultaneously minimizing the drawbacks of both. Dual- or multi-modality sensors is the collaborative association of two or more detection methods, enabled by single or multi modal

78 probes which ensures enhanced detection sensitivity and better reliability of collected
79 data.(Chuong et al., 2017; Peng et al., 2019; Xiong et al., 2018) Therefore, instead of
80 developing conventional single modality sensors, in the present research, we have worked on
81 engineering the dual-modality biosensor.

82 Recent developments on preparing multifunctional nanomaterials enhance the
83 detection methodology and also allow the possibility of changing from single modality to a
84 dual-modality detection methods.(Chowdhury et al., 2018; Xiong et al. 2018; Ganganboina et
85 al., 2018b; Ganganboina and Doong 2020) Nanomaterials with inherent activity similar to
86 enzymes probe the possibility of replacing specific enzymes like peroxidase and catalase,
87 etc.(Ganganboina and Doong 2018; Ye et al. 2017) V_2O_5 is considered as artificial enzyme
88 (nanozyme) attributing to the unique advantages like immense catalyticity, robust stability,
89 and facile surface reformation.(Vernekar et al., 2014) Liposomes are an attractive approach
90 owing to their versatile and unique properties which facilitate the encapsulation of
91 nanomaterials, thereby amplifying the detection signal.(Carboni et al., 2019) The
92 encapsulated probes remain protected and almost inactive inside the liposome which can
93 reduce the background noise significantly. Various reports demonstrated the colorimetric or
94 fluorometric responses in the presence of a target protein using liposome conjugated natural
95 and synthetic lipids.(Holme et al., 2018) Chowdhury et al. prepared the Sphingomyelinase
96 enzyme responsive liposome based release of methylene blue and established a quantitative
97 relationship between the amount of target enzyme and released methylene blue. On the other
98 hand, magnetic susceptibility of MNPs is being widely used for the magnetic separation and
99 enrichment of biomolecules, like viruses, under externally applied magnetic fields, helping in
100 exclusive specificity and reducing the background signal noise.(Oh et al., 2018; Xiong et al.
101 2018)

In light of the advantages of the artificial enzyme-based signal amplification, liposome based encapsulation techniques and magnetic separation we desired to develop a robust sensing method with dual-modality. Herein, using V_2O_5 NPs-encapsulated liposomes (VONP-LPs), an ultrasensitive virus sensing method with electrochemical and colorimetry combined dual-modality read out sensor is developed. To separate the target virus from the medium, the well-established MNPs have been used. VONP-LPs as well as MNPs were functionalized with antibody specific to NoV. In addition of various concentration of NoV-LPs or NoV, VONP-LPs and MNPs bind to NoV-LPs and make a sandwich-like structure. The nanoconjugate of VONP-LPs, NoV-LPs and MNPs is magnetically separated from its analyte medium and then lysed out the encapsulated V_2O_5 from the liposome. As large number of encapsulated V_2O_5 NPs are released from captured liposomes even at low virus concentration, electrochemical signal using DPV and colorimetric signal in response to oxidized 3,3',5,5'-Tetramethylbenzidine (TMB) can be amplified significantly (**Scheme 1**). The developed biosensor illustrates its ability to detecting NoV-LPs in a broad range with low detection limit at fg mL^{-1} level attributing to its profound architecture, easy manipulation, and facile storing of V_2O_5 NPs.

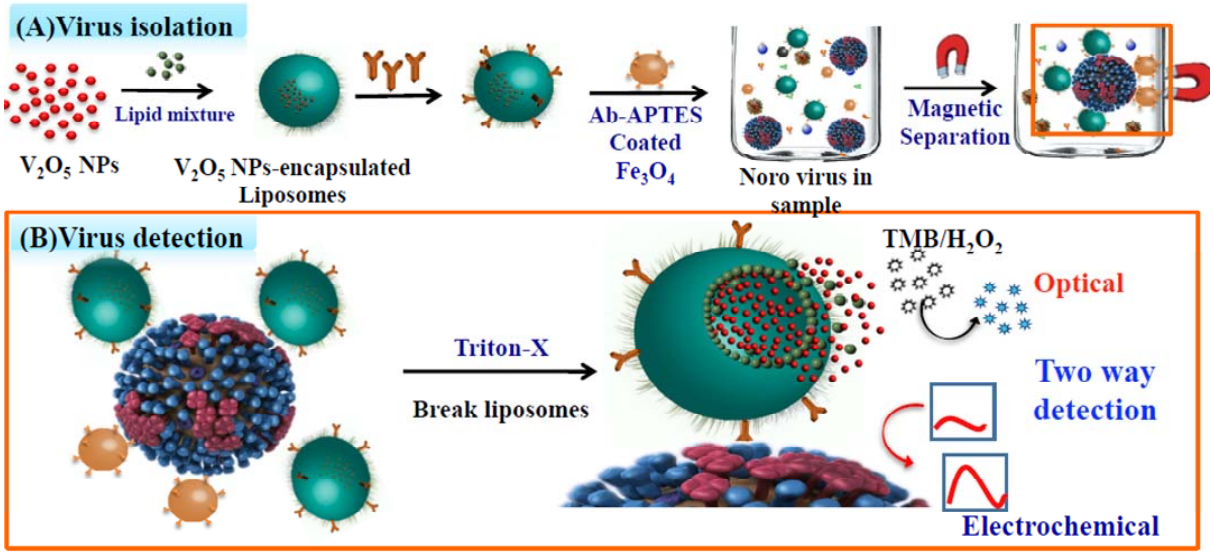

118
119 **Scheme 1.** Schematic representation illustrating the fabrication process of V_2O_5 NPs-
120 encapsulated liposomes (VONP-LPs) (**A**) and NoV detection principle (**B**). The V_2O_5 NPs
121 released from captured liposomes act as effective peroxidase mimics to catalyze chromogenic
122 substrates and generate electrochemical redox signal.

123

124 **2. Materials and methods**

125 Chemicals, Preparation of V_2O_5 Nanoparticles (V_2O_5 NPs),(Pan et al., 2015) APTES
126 Coated MNPs, (Ganganboina et al., 2017a) V_2O_5 NPs-Encapsulated Liposome (VONP-LPs),
127 (Sharmin et al., 2016) Characterizations, Peroxidase-like Catalytic Activity of V_2O_5 NPs, (Ku
128 et al., 2017) Preparation of Anti-NoV antibody-conjugated VONP-LPs, (Ahmed et al., 2017)
129 MNPs, NoV-LPs and Clinically Isolated NoV and Detection of NoV-LPs and norovirus
130 protocols can be found in the Supplementary data.

131

132 **3. Results and discussion**

133 *3.1 Working principle.*

Scheme 1 exhibits the essential principal of the newly developed dual-modality sensing method for robust and ultrasensitive detection of NoV. It comprises of V_2O_5 NPs-encapsulated liposomes (VONP-LPs) and MNPs conjugated with anti-NoV antibodies, which can specifically recognize the NoV and can form sandwich like structure as depicted in the **scheme 1**. In thus formed sandwich like structure with VONP-LPs/virus/MNPs, anti-NoV antibody-conjugated MNPs separate the target virus, and VONP-LPs amplify the signal. Following the interaction, the nano conjugates of VONP-LPs/virus/MNPs are separated magnetically from the excess reagents and other interfering substances. Thereafter the successfully separated VONP-LPs/virus/MNPs are treated with Triton X surfactant for the release of the encapsulated V_2O_5 NPs which act as catalyzer accelerating the oxidation of TMB by H_2O_2, leading to the production of colorimetric signals to quantify viruses by indirect calibration. The absence of virus cannot form the nanoconjugate and bare accumulation of MNPs after magnetic separation resulting in insufficient oxidation of TMB for generating colorimetric signal and redox reaction for the DPV signal.

As we know, the electrochemical signal is more sensitive, we further used the electrochemical modality for highly sensitive detection and precise diagnosis of NoV. The released V_2O_5 NPs from captured liposomes, are also used for electrochemical signal generation based on DPV signal generated by V_2O_5 NPs. The solution containing magnetically isolated VONP-LPs/virus/MNPs, after treating with Triton X surfactant for the release of the encapsulated V_2O_5 NPs was deposited on the graphene coated GC electrode. The V_2O_5 NPs enhance the redox signal in DPV spectrum and the redox signal of V_2O_5 NPs at 0.46 V increases in accordance with virus concentration, providing excellent sensitivity and selectivity for quantitative detection of NoV. The developed dual-modality sensor will provide two signal readouts in one analytical system, leading in superior accuracy, diversity, and flexibility to fulfil the detection needs at diverse regions and diverse circumstances.

Dual-modality signal readout and magnetic separation of virus avail the detection ability in sample with low concentration analytes and complex systems.

3.2. Characterizations of V_2O_5 NPs and VONP-LPs

V_2O_5 NPs with lateral dimension of up-to tens of nanometers that are novel materials for nanozymes are produced using hydrothermal process.(Ganganboina and Doong 2018) The morphology and structure of the as-prepared V_2O_5 NPs is systematically examined. **Fig. 1a** shows the typical TEM images of the V_2O_5 NPs with quasi spherical in shape and homogeneous distribution. The HR-TEM image of single V_2O_5 NP in **Fig. 1b** clearly shows the lattice fringes with inter spacing distance of 0.34 nm, corresponding to (110) planes of V_2O_5.(Ganganboina et al., 2017b) **Fig. 1c** shows the particle size distribution of V_2O_5 NPs in the range of 15 – 40 nm with average lateral size of 25 ± 1.5 nm. Corresponding narrow-distributed particle size with good uniformity allows considerable improvement in the sensing properties.

To confirm the structural properties of the V_2O_5 NPs, XRD analysis is performed and shown in **Fig. 1d**. The XRD patterns of V_2O_5 NPs show several peaks centered at 15.33°, 20.34°, 21.19°, 26.1°, 31.11° and 32.3° 2θ, which can be indexed as (001), (002), (110), (101), (011), and (301) planes of orthorhombic phase of V_2O_5.(Ganganboina and Doong 2018) To detect the elemental species and the oxidation state of V_2O_5 NP, XPS spectrum is analyzed. The survey spectrum of V_2O_5 NPs (**Fig. 1e**) shows peaks at 284.2, 517, 525 and 531 eV, which can be attributed to the spectra of C 1s, V 2p and O 1s, indicating the successful preparation of V_2O_5.(Ganganboina et al. 2017b) The XPS spectrum of V 2p peak is further deconvoluted to understand the oxidation state of vanadium element in V_2O_5. As shown in **Fig. 1f**, the deconvoluted peak of V 2p exhibits two peaks positioned at 517.3 eV

and 524.7 eV, that are representative peaks of V^{5+} $2p_{3/2}$ and V^{5+} $2p_{1/2}$, validating the V^{5+} state in V_2O_5 NPs.(Ganganboina and Doong 2018)

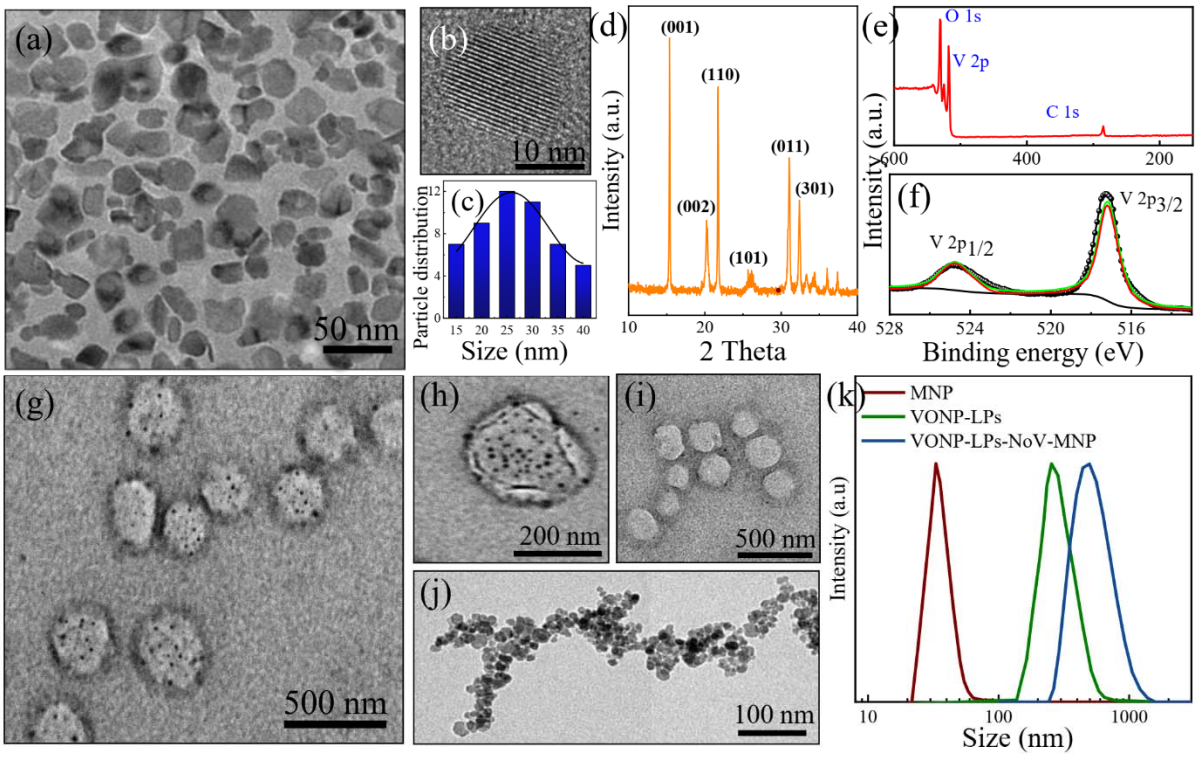

Fig.1 Characterizations of V_2O_5 NPs, liposomes encapsulated V_2O_5 nanoaprticles and MNPs. (**a**) TEM image, (**b**) HR-TEM image, (**c**) particle size distribution (**d**) XRD pattern, (**e**) XPS survey spectra, (**f**) deconvoluted XPS spectra of V 2p of as-synthesized V_2O_5 NPs. TEM images of (**g, h**) the V_2O_5 NPs-encapsulated intact liposomes under different magnifications, (**i**) liposome without loading of V_2O_5 NPs, (**j**) MNPs and (**k**) DLS measurement to verify the particle sizes of various components of V_2O_5 encapsulated liposome based dual-modality biosensor.

We synthesized the V_2O_5 NPs incorporated liposomes (VONP-LPs) using the lipid film hydration and membrane extrusion method. VONP-LPs assembled from a mixture of

DOPC, DOPG and DSPE (50:30:10), encapsulating V_2O_5 NPs in the liposome formulations. The formation of VONP-LPs is verified using transmission electron microscopy (**Fig. 1g** and **h**). VONP-LPs are spherical in structures with homogeneous distribution and an average diameter of around 200 nm. The loading of V_2O_5 NPs in the liposome is confirmed by TEM image in **Fig. 1h**, which clearly shows the incorporated V_2O_5 NPs inside the liposome. As a reference, TEM image of bare liposomes without incorporating V_2O_5 NPs is shown in **Fig. 1i**. As shown in **Fig. 1j**, the MNPs prepared by coprecipitation method are spherical with diameters in the range of 10–15 nm. The hydrodynamic radius of nanomaterials before and after formation of immune complex is determined using dynamic light scattering (DLS). Average particle size of the as synthesized MNPs and VONP-LPs is found of 35 (PDI 0.3) and 300 nm (PDI 0.27), respectively (**Fig. 1k**). After the formation of VONP-LPs/virus/MNP nanoconjugate, the size of the nanoconjugate increased to 500 nm, indicating the successful formation of the sandwich structure. The TEM image of the sandwich structure of VONP-LPs, MNPs and NoV after staining the virus with urinyl acetate is shown in Fig. S1 of supplementary data. The viruses bound with the MNPs are clearly visible in the image whereas the VONP-LPs are not visible due to its less mass compared with others.

3.3. Peroxidase-like catalytic activity of V_2O_5 NPs.

We quantified the peroxidase-like activity of V_2O_5 NPs using steady-state kinetic assay. The catalysis of peroxidase substrates TMB by H_2O_2 is chosen as a standard catalytic reaction.(Oh et al. 2018) Following the activity of peroxidase, V_2O_5 acted as the catalyst in the oxidation of TMB with H_2O_2, forming a blue colored complex with absorbance at 653 nm (**Fig. 2a**). Without the presence of V_2O_5, the reaction between TMB and H_2O_2 was slow and not obvious compared to the reaction with V_2O_5 (**Fig.e 2b**). To show the V_2O_5 was involved

in the reaction as the nanozyme with catalytic activity, the reaction was monitored with the function of time in seconds. Increasing concentration of V_2O_5 was applied to the chromogen solution, TMB and H_2O_2, and the charge-transfer complex was measured in absorbance (**Fig. 2c**). The absorbance of the product was calculated as the TMB concentration by referring to the Beer-Lambert law and the molar extinction coefficient of TMB (36,000 M^{-1} cm^{-1}). Next, the reaction rate which was calculated based on the linearity line of product concentration vs time, was plotted as the function of concentration of V_2O_5 (**Fig. 2d**), showing the linearly proportional increment of the reaction rate to the concentration of V_2O_5. This showed the V_2O_5 in the reaction acted as the nanozyme rather than the substrate.

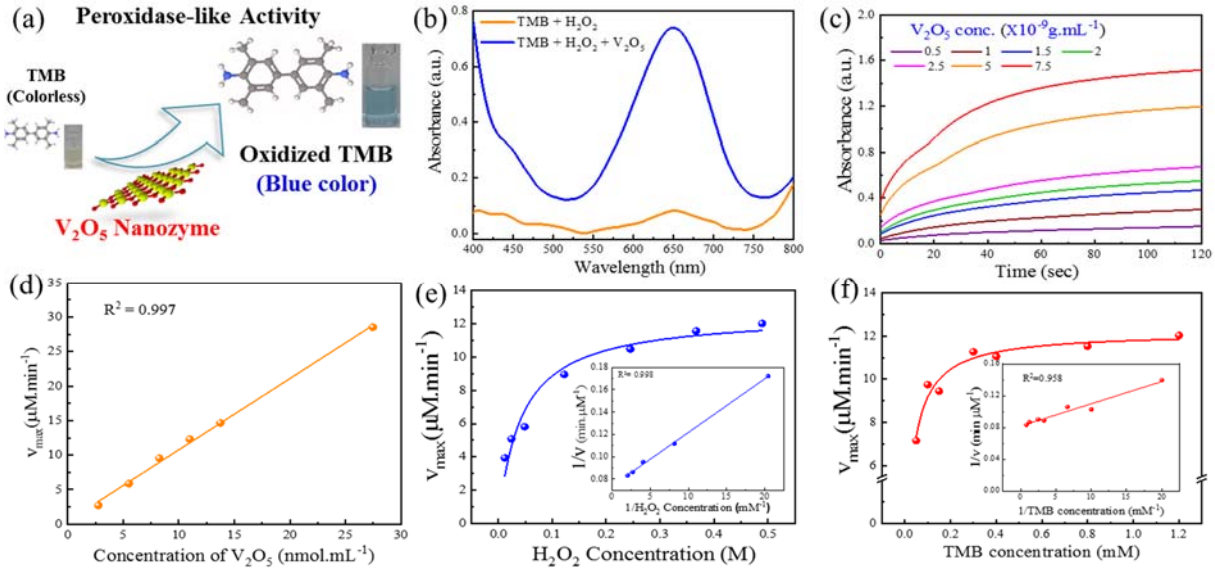

Fig. 2 Peroxidase-like catalytic activities of V_2O_5 NPs for oxidation of TMB with H_2O_2 to produce blue colored complex. (**a**) Schematic representation, pictures and (**b**) UV−vis spectrum of the blue colored complex of oxidized TMB catalyzed by V_2O_5 NPs. (**c**) V_2O_5 NP concentration and time dependent changes in absorbance at 653 nm for TMB−H_2O_2 reaction, (**d**) initial reaction velocity of TMB oxidation under V_2O_5 NPs. The Michaelis−Menten

kinetic curves of V_2O_5 NPs at various concentrations of H_2O_2 (**e**) and TMB (**f**) and inset with double-reciprocal plots of activities.

In this work, the steady-state kinetic parameter of the V_2O_5 as the nanozyme to the catalytic reaction substrate, TMB and H_2O_2, was determined by independently varying the substrate concentration. Like the concentration-dependent assay, regular Michaelis Menten curves are acquired by plotting the initial reaction rate in the linear part of the absorbance vs time, against the concentrations of H_2O_2 (**Fig. 2e**) and TMB (**Fig. 2f**). The double-reciprocal plot (Lineweaver-Burk plot) is shown in the inset of the respective figures to show the linearity of the inverse of the Michelin-Menten plot. The K_m and V_{max} of H_2O_2 and TMB of the V_2O_5 are shown in the supplementary Table S1. Based on the V_2O_5 concentration used in the assay (27 μM), the catalytic efficiency ($k$cat/km) of H_2O_2 and TMB was calculated about 322.59 $M^{-1}s^{-1}$ and 608.14 $M^{-1}s^{-1}$ respectively. This showed higher affinity and more efficient catalytic interaction of the V_2O_5 is initiated by one substrate in the catalytic performance.

3.4. Feasibility of NoV-LP detection using VONP-LPs.

Metal oxides based signal amplification approach is extensively used to develop colorimetric and electrochemical methods for ultrasensitive virus detection.(Gao et al., 2019) Based on the VONP-LPs, electrochemical redox probe and peroxidase-like activity, a dual-modality sensor is developed for NoV detection. As synthesized V_2O_5 NPs exhibited both electrochemical redox activity and peroxidase-like activity. The electrochemical performance of V_2O_5 NPs was evaluated using the cyclic voltammetry. **Fig. 3a** shows the CV curves of V_2O_5 NPs, graphene and V_2O_5 -graphene in 0.1 M H_2SO_4 solution in the potential window of

0 to 0.8 V at a scan rate of 10 mV s^{-1}. A pair of reversible redox peaks at around 0.46 V and 0.21 V is presented in the CV of V_2O_5 NPs containing electrodes, indicating their redox behavior. The graphene coated gold electrode increased the intensity of V_2O_5 NPs redox peaks attributing to the conductive and capacitive properties when the graphene is coated on gold electrode. In addition, two-dimensional property of graphene may allow the released V_2O_5 NPs to retain on the surface of graphene because of π-π stacking interaction, allowing the increase in redox signals intensity. To obtain the utmost response from the released V_2O_5 NPs, a graphene-coated gold electrode is used as working electrode.

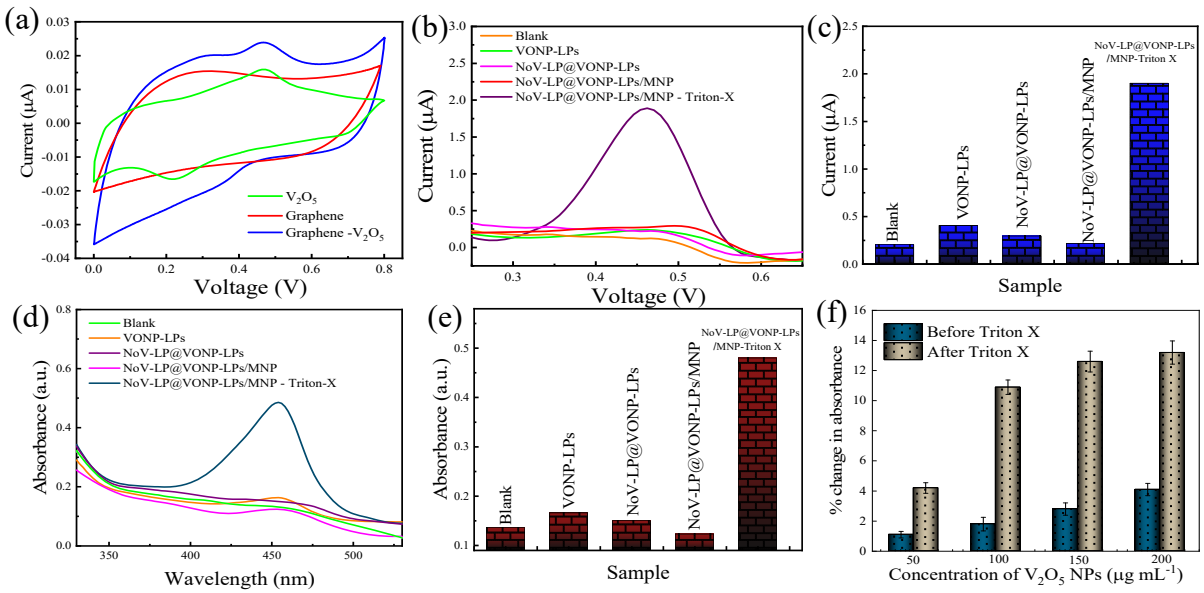

Fig. 3. Demonstration of electrochemical and colorimetry based dual-modality detection method. (**a**) Cyclic voltammetry of V_2O_5 and graphene, (**b**) DPV curves of individual materials of V_2O_5 NPs encapsulated liposome based sensing, (**c**) response of current against individual component of sensor, (**d**) absorbance curves of individual materials of V_2O_5 NPs encapsulated liposome based sensing, (**e**) change in absorbance intensity in response to individual component of sensor and (**f**) effect of V_2O_5 NPs loading concentration of 50,100,150 and 200 μg mL^{-1} in presence of 10 pg mL^{-1} NoV-LPs.

In addition, to verify the electrochemical efficiency of V_2O_5 NPs released from encapsulated liposomes, the sensing procedure is evaluated using the DPV in the presence of 100 pg mL^{-1} NoV-LPs. As V_2O_5 NPs exhibit the redox peaks at 0.46 V, a potential window from 0.25 – 0.65 V is used for measuring DPV. As shown in **Fig. 3b**, ignorable influence on the change in DPV signal in noticed on addition of liposomes (orange). Likewise, the addition of NoV-LP-bound VONP-LPs (purple) and sandwich structure of NoV-LP-bound VONP-LPs and MNPs (pink) on the graphene coated GC electrode also doesn't exhibit any redox peaks, confirming that the V_2O_5 NPs are inside the liposomes and, therefore, unable to produce redox signal. Interestingly, upon addition of triton-X to the magnetically separated nanoconjugate of VONP-LPs@NoV-LPs/MNPs, an obvious redox peak appears at 0.46 V (blue line), majorly assigned to the V_2O_5 NPs released from captured liposomes. This phenomenon also can be seen in the **Fig. 3c**, maximum current obtained only after the addition of triton X to the magnetically separated nanoconjugate of NoV-LP, VONP-LPs and MNPs confirming the DPV signal generated only by the released V_2O_5 NPs. To understand the significance of VONP-LPs in signal amplification, bare V_2O_5 NP, conjugated with the antibody, are used instead of VONP-LPs for sensing NoV-LPs. It is expected that V_2O_5 NP also offer the similar mechanism for the detection of NoV-LPs, anticipating that a single virus particle can only attach with a single V_2O_5 NP whereas a single liposome can release multiple number of V_2O_5 NP, amplifying the signal significantly. The comparison sensing data using V_2O_5 NP and VONP-LPs is shown in the **Fig. S2** of Supplementary data. It can be clearly seen that 1000-fold detection sensitivity is achieved by using the VONP-LPs clearly demonstrating the significance of liposomal encapsulation in developed dual modality sensor **Fig. S3.** in supplementary data shows the control sensing experiment using MNPs and VONP-LPs with and without antibody-conjugation is performed. It can be clearly observed that only 4% change in current response is obtained when nanomaterials are not conjugated

with antibody in comparison with nanomaterials conjugated with antibody. These results clearly demonstrate the negligible non-specific binding of norovirus with nanomaterials used in the developed sensor.

In addition simultaneously, colorimetric change obtained by the individual nanomaterials of the biosensor is also monitored using the TMB oxidation in presence of H_2O_2. In corroboration with the above results VONP-LPs, NoV-LP-bound VONP-LPs and nanoconjugate of VONP-LPs@Nov-LPs/MNPs have produced very less change in UV-visible spectra as shown in **Fig. 3d**. Addition of triton-X to nanoconjugate of VONP-LPs, NoV-LPs and MNPs solution, results in a strong absorption peak at 450 nm attributed to the oxidation of TMB by released V_2O_5 NPs from the captured liposomes. This phenomenon confirms the negligible catalytic activity of V_2O_5 NPs present inside the liposome confirming the encapsulated probes remain protected and almost inactive inside the liposome which can reduce the background noise significantly. Thus obtained results affirm the developed sensing method has excellent feasibility and reliability. The multicomponent integrated sensor can efficaciously enhance the sensitivity of developed method, resulting robust and sensitive detection of the NoV.

In addition, the optimal loading concentration of V_2O_5 NPs inside the liposome was evaluated. During the hydration of liposomes, various V_2O_5 NPs solutions of 50, 100, 150 and 200 μg mL^{-1} are used to obtain liposomes encapsulated with different V_2O_5 NPs concentration and then tested for NoV-LPs detection. As shown in **Fig. 3f**, it is evident that excluding 50 μg mL^{-1} all other concentrations of V_2O_5 NPs show significant absorbance and DPV response. As the concentration of the target virus should be low enough, it is highly desirable to load maximum amount of V_2O_5 NPs inside the liposome for low level detection, making the smallest amount used 50 μg mL^{-1} not to be continued. Compared with other three concentrations of V_2O_5 NPs encapsulated liposomes, the overall absorbance intensity of 100

μg mL^{-1} is quite comparable with the 150 and 200 μg mL^{-1} concentration however with low background signal. As the high concentration of V_2O_5 NPs encapsulated liposomes are difficult to purify and the 100 μg mL^{-1} V_2O_5 NPs encapsulated liposome also provide sufficient signal, we have selected this concentration as optimum for further studies.

3.5. Specificity and sensitivity of NoV-LP with dual-modality readout

To determine the linear range and sensitivity of the developed dual-modality sensor, different concentrations of NoV-LPs are examined. Anti-NoV antibody-conjugated VONP-LPs, MNPs and aliquot of NoV-LPs with various concentrations are mixed. VONP-LPs and the MNPs are bound with NoV-LPs through the specific interaction with antibody on their surface and a nanoconjugate of VONP-LPs, NoV-LPs and MNPs is formed. Thus formed nanoconjugate is washed for three times using PBS and magnetic separation. The isolated nanoconjugate releases the encapsulated V_2O_5 NPs after the disruption of the liposomes triggered by the surfactant, Triton X.(de Matos et al., 2019) A working solution containing mixture of TMB and H_2O_2 is added above mixture and incubated at 25°C, following the change of solution to blue color. TMB oxidation reaction was stopped by adding 10% H_2SO_4 solution and absorbance was recorded.(Oh et al. 2018) As shown in **Fig. S4** (Supplementary data) the color of the above solution slowly changed to dark blue with the increasing concentration of NoV-LPs. V_2O_5 NPs released form the disrupted liposomes, catalyzed oxidation of different amount of TMB, thereby resulting in this colorimetric change. After the addition of 10% H_2SO_4 solution the intensity of UV-vis peak at 450 nm for final solutions with various colors increased with respect to the increasing concentration of NoV-LPs (**Fig. 4b**). An excellent linear correlation occurred from 1 pg mL^{-1} to 100 ng mL^{-1} with an R^2 of 0.988 by drawling the calibration curve using the change in absorbance intensity and NoV-

LPs concentration (**Fig. 4c**). In addition, the limit of detection (LOD), as determined by the 3σ/S(Ganganboina and Doong 2019) (S is the slope of linear calibration plot and σ is the standard deviation of the lowest signal) is 0.34 pg mL^{-1}.

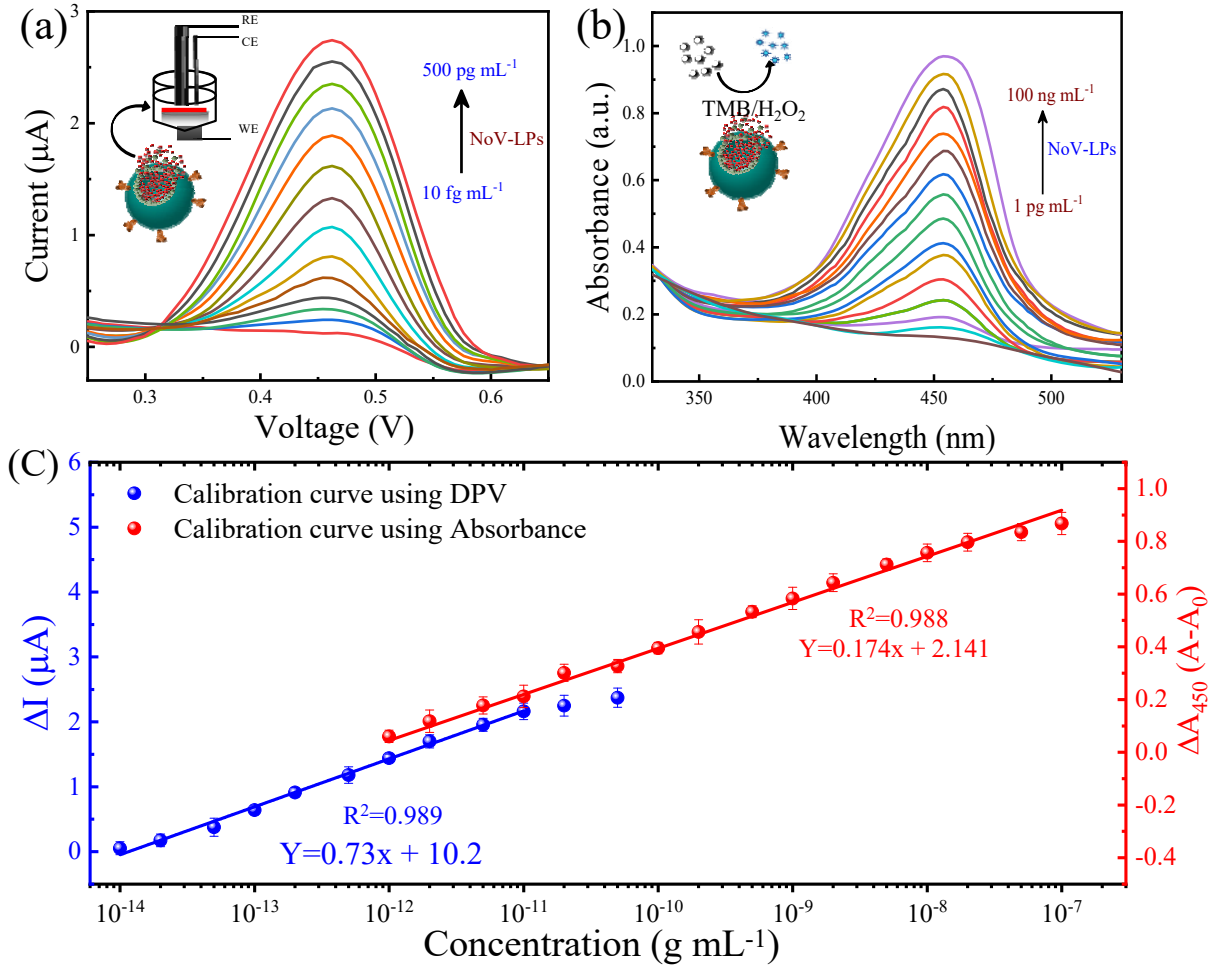

Fig. 4. Sensitivity test of V_2O_5 NPs encapsulated liposomes based dual-modality sensor for NoV-LPs sensing. (a) DPV, (b) absorbance spectra of different concentrations of NoV-LPs and (c) dual-modality calibration curve for detection of the NoV-LPs, change of current intensities and absorbance peak intensity vs concentration of NoV-LPs.

As known, the electrochemical signal is highly sensitive comparision with absorption signal of TMB oxidation, allowing usage of the electrochemical modality for ultrasensitive sensing and prevising detection. As anticipated, the electrochemical signal can be measured in the existence of very low concentration of NoV-LPs. The solution containing V_2O_5 NPs released from the disrupted liposomes was dropped on to the graphene coated Au electrode to check the DPV response. **Fig. 4a** shows that the DPV response at around 0.46 V are increased with increasing concentration from 10 fg mL^{-1} to 500 pg mL^{-1} of NoV-LPs. Correlation coefficient (R^2) of 0.989 is obtained in the linear range of NoV-LPs from 10 fg mL^{-1} to 10 pg mL^{-1} (**Fig. 4c**). The limit of detection (LOD) was calculated to be 4.1 fg mL^{-1} as determined by the 3σ/S. Ashiba et. al 2017, have calculated the mass of a single NoV-LP by considering the VLP structure and the mass of their individual protein components. According to their study, 10 pg mL^{-1} of VLP accounts to be 4.3×10^5 particles mL^{-1}. Utilizing this information, the LOD of this study in optical method is 0.34 pg mL^{-1}, which accounts to ~10^4 particles mL^{-1} and in electrochemical method it is 4.1 fg mL^{-1} equivalents to ~10^2 particles mL^{-1}. The sensitivity of the developed dual-modality sensor for NoV-LPs detection is competitive with recently developed sensing methods comprising electrochemical(Baek et al., 2019; Chand and Neethirajan 2017; Hong et al., 2015; Hwang et al., 2017) and optical(Batule et al., 2018; Han et al., 2018; Khoris et al., 2019; Nasrin et al. 2018) methods (**Table S2 of Supplementary data**). These results indicated that the developed dual-modality sensor for NoV-LPs detection exhibits benefits including ultrasensitivity of electrochemical method, excellent quantitative ability and wide linear range detection allowing it to be applied not only for handy initial screening, but also exact detection of viral disease.

3.6. Effect of complex matrix on dual-modality sensor for NoV detection

To evaluate the applicability of the developed dual-modality sensor in sophisticated biological sample matrix, 10% human serum is used as detection medium. NoV-LPs spiked samples with various concentration shows a similar trend of detection confirming the application of the developed sensor for the clinical sample monitoring. Calibration curve obtained for NoV-LPs sensing using 10% human serum as detection medium is shown in **Fig. 5a**. The slope of linearity is slightly flattened in comparision with the calibration curve obtained in DI water samples. In addition detection of NoV-LPs in 50% diluted and 100% serum is also performed (Fig. S5 of supplementary data). The slope of the calibration curves for NoV-LPs obtained using 50% diluted and 100% serum are severely flattened in comparision with the calibration curve obtained in 10% diluted serum as detection medium. Therefore to reduce the interference caused by the complex serum matrix, 10% diluted serum has been chosen to perform the analysis of NoV-LPs spiked serum samples. The complex human serum matrix resulted in slight reducing of the slope of the calibration curve, resulting in declining the LOD value to 8.1 fg mL^{-1} and 0.75 pg mL^{-1} in electrochemical and colorimetric modality. However, the sensitivity of the developed method in serum matrix is fairly considerable in comparision with other reports for its real application.

3.7. Clinical NoV detection using dual-modality sensor.

Above results confirmed the ultra sensitivity and excellent specificity of the VONP-LPs based dual-modality biosensor proving applicability of developed sensor for real samples (**Fig. 5b)**. To confirm the practicability real clinical samples are examined. Different types of clinical NoV (GII. 2, GII. 3, GII.4) from human feces of infected patients are detected using the developed dual-modality sensor. For NoV type GII.2, GII.3 and GII.4, the intensity of DPV signal continuously increased with the increase in concentration of NoV from 10^2 to 10^4

RNA copies mL^{-1} and intensity of absorbance signal increased from 10^4 to 10^7 RNA copies mL^{-1}. GII.2 and GII. 3 showed a correlation coefficient (R^2) of 0.978 and 0.963 in absorbance modality and (R^2) 0.961 and 0.954 in electrochemical modality. GII.4 exhibits relatively lower correlation coefficient (R^2) of 0.945 and 0.935 in absorbance and electrochemical modality respectively compared to other two. The LOD for GII. 2 is measured to be 81 RNA copies mL^{-1} and 72 RNA copies mL^{-1} for GII.3.

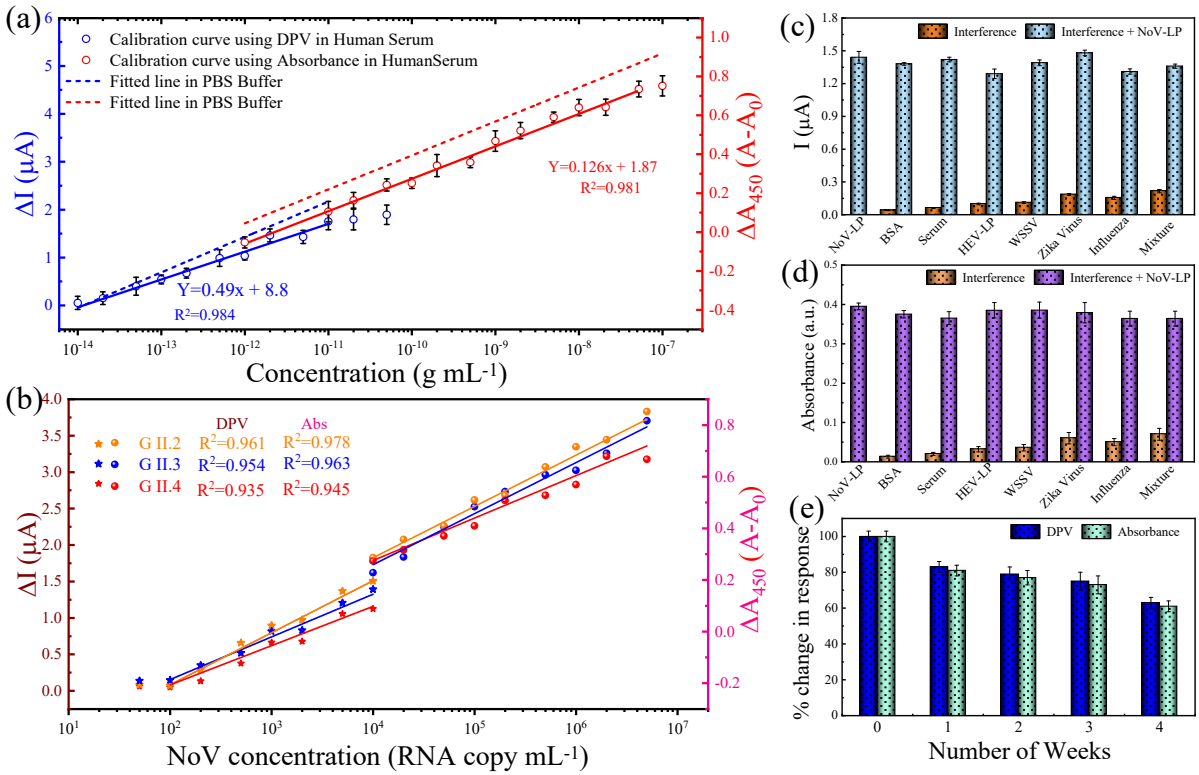

Fig. 5. Effect of sample matrix, detection of clinical samples, specificity and stability of dual-modality biosensor for NoV detection. (**a**) Calibration curve for NoV-LPs using in 10% human serum as sensing medium and its corresponding calibration line (dotted line) onbtained in DI water, (**b**) calibration curves for detection of clinically isolated NoV (genotype II.2, 3 and 4) in concentration range from 10^2 to 10^6 copies mL^{-1}. Change in (**c**) current intensity, (**d**) absorbance intensity of VONP-LPs and MNP system in the presence of the target NoV-LPs and other common interferences, (**e**) Stability test of the VONP-LPs and

MNP with 10^5 copies mL^{-1} of NoV showing percentage change in DPV (blue bars) and absorbance (light blue) over 4-week period.

3.8. Specific and stable dual-modality sensor.

The selectivity of the developed VONP-LPs based immunoassay for NoV detection is next evaluated. BSA, serum, HEV-LPs, WSSV, Zika virus and influenza virus are used as negative samples to examine the specificity through comparing the electrochemical response to 10 pg mL^{-1} NoV-LPs and optical response to 1 ng mL^{-1} NoV-LPs. **Fig. 5c** shows the current response of developed immunosensor to the mixture of negative samples and NoV-LP. Increased current intensity is observed in the NoV-LPs sample and no obvious change is observed in the other samples. Only small increase in current intensity 0.5 – 10% in negative samples compared with the NoV-LPs is observed clearly indicating the superior specificity of VONP-LPs based sensor towards NoV-LPs sensing. The selectivity of the developed sensor for NoV-LPs is also measured by colorimetric modality. Blue color can be observed only in the presence of target NoV-LP (**Fig. 5d**). Because the interfering samples are unable to link the conjugation of VONP-LPs, MNPs. As a result, after separation, there are no V_2O_5 NPs to catalyze the TMB oxidation to form blue color product. These results show that the developed dual-modality sensor is highly specific for NoV-LP detection.

Good storage stability of VONP-LPs based sensor for NoV detection is required to assure the reliability of the developed method. To examine the stability of the sensor, the NoV sensing was performed repeatedly over 1-month period as shown in **Fig. 5e**. Though the individual components of VONP-LPs and the MNPs are preserved at 4°C, the degradation of the liposome and the effectivity of the antibody have shown some degradation over time, resulting a noteworthy decrease in performance within its 1st week of storage. However the

sensor can be appreciable for usage up to the 3rd week of storage. After that, due to the obvious degradation of antibody, the DPV and absorbance signal decrease relatively make the system less reliable and unable to use.

In comparison with regular single modality assay, dual-modality sensor using VONP-LPs exhibit the below benefits. In this dual-modality sensor absorbance and electrochemical sensing modalities are merged into single sensing system, benefiting the wide linear range sensing using colorimetric signal and electrochemical signal with significantly enhanced sensitivity. V_2O_5 NPs exhibit high catalytic efficiency in comparision with natural enzymes, providing increased color signal. The loading ability of V_2O_5 NPs into liposomes is increased by utilizing the large interior 3D space of liposomes as cargo holders. V_2O_5 NPs inside the liposomes reduces the loss of catalytic and redox efficiency which may be incurred by chemical conjugation. Further, usage of MNPs for separating the virus from the strong sample matrix allows negligible background noise and may help in exhibiting strong anti-interference ability and accuracy. Finally, the developed dual-modality sensor avoids the complicated sample preparation and limits the use of sophisticated analytical equipment making the detection method simple and fast.

4. Conclusions

In this study, we have prepared a dual-modality signal biosensor based on V_2O_5 NPs encapsulated liposomes (VONP-LPs) for ultrasensitive detection of virus. The VONP-LPs bound to virus and enriched by magnetic separation could be hydrolyzed by triton X allowing the release of encapsulated V_2O_5 NPs. Released V_2O_5 NPs act as nanozyme for the oxidation of TMB, producing amplified colorimetric signal and also induce the electrochemical redox signal monitored by DPV. Utilizing the superiority of dual-modality sensor with two

quantitative analysis forms, norovirus like particles (NoV-LPs) were detected by electrochemical signals in a linear range of 10 fg mL^{-1} to 10 pg mL^{-1} with a detection limit down to 4.1 fg mL^{-1}. Using the colorimetric signal readout, quantitative discerning of NoV-LPs was estimated in a broad range from 1 pg mL^{-1} to 100 ng mL^{-1} with a limit of detection down to 0.34 pg mL^{-1}. Additionally, clinically isolated NoV from infected patients also successfully assayed where the detection limit was found as 72 RNA copies mL^{-1}. The comparative higher detection limit in optical measurement is a strong limitation of this method as the sensor could not get the dual confirmation in the most crucial low concentration range from pg to fg mL^{-1}. A possible replacement of TMB-based colorimetric method with fluorometric method with the can be a good alternative for the future study. Summarizing the overall outcomes, this dual-modality method draws a good capability in the complex matrix, for both colorimetry and electrochemical signal based convenient and ultrasensitive diagnosis of infections clinical diagnosis and disease treatment in virus-affected areas.

Acknowledgement

We thank for Professor Masakazu Yamazaki of Research Institute of Electronics, Shizuoka University for kind instruction of liposome preparation. A.B.G. and A.D.C. sincerely thanks the Japan Society for the Promotion of Science (JSPS) for a postdoctoral fellowship (Grant Nos. 19F19064 and 17F17359).

Supplementary data

Supplementary data associated with this article can be found in the online version at:

494

495 **ORCID**

496 Enoch Y. Park: 0000-0002-7840-1424

497 Akhilesh Babu Ganganboina: 0000-0003-3259-5080

498 Ankan Dutta Chowdhury: 0000-0002-6391-5895

499

500 **References**

501 Ashiba, H., Sugiyama, Y., Wang, X., Shirato, H., Moriguchi, K, H., Taniguchi, K., Ohki, Y.,
502 Fukimaki, M., 2017. Biosens. Bioelectron. 93, 260-266.
503 Ahmed, S.R., Takemeura, K., Li, T.-C., Kitamoto, N., Tanaka, T., Suzuki, T., Park, E.Y.,
504 2017. Biosens. Bioelectron. 87, 558-565.
505 Anusha, J., Kim, B.C., Yu, K.H., Raj, C.J., 2019. Biosens. Bioelectron. 142, 111511.
506 Baek, S.H., Kim, M.W., Park, C.Y., Choi, C.S., Kailasa, S.K., Park, J.P., Park, T.J., 2019.
507 Biosens. Bioelectron. 123, 223-229.
508 Batule, B.S., Kim, S.U., Mun, H., Choi, C., Shim, W.B., Kim, M.G., 2018. J. Agric. Food.
509 Chem. 66(11), 3003-3008.
510 Bhardwaj, J., Sharma, A., Jang, J., 2019. Biosens. Bioelectron. 126, 36-43.
511 Bui, M.-P.N., Ahmed, S., Abbas, A., 2015. Nano Lett. 15(9), 6239-6246.
512 Carboni, V., Maaliki, C., Alyami, M., Alsaiari, S., Khashab, N., 2019. Advanced
513 Therapeutics 2(4), 1800085.
514 Chand, R., Neethirajan, S., 2017. Biosens. Bioelectron. 98, 47-53.
515 Chowdhury, A.D., Ganganboina, A.B., Tsai, Y.C., Chiu, H.C., Doong, R.A., 2018. Anal.
516 Chim. Acta 1027, 109-120.

517 Chowdhury, A.D., Takemura, K., Li, T.-C., Suzuki, T., Park, E.Y., 2019. Nat. Commun.
518 10(1), 1-12.
519 Chuong, T.T., Pallaoro, A., Chaves, C.A., Li, Z., Lee, J., Eisenstein, M., Stucky, G.D.,
520 Moskovits, M., Soh, H.T., 2017. Proc. Natl. Acad. Sci. U.S.A 114(34), 9056-9061.
521 De Matos, M.B., Miranda, B.S., Rizky Nuari, Y., Storm, G., Leneweit, G., Schiffelers, R.M.,
522 Kok, R.J., 2019. J. Drug Targeting, 2019 27(5-6), 681-689.
523 Dutta Chowdhury, A., Ganganboina, A.B., Nasrin, F., Takemura, K., Doong, R.A., Utomo,
524 D.I.S., Lee, J., Khoris, I.M., Park, E.Y., 2018. Anal. Chem. 90(21), 12464-12474.
525 Faria, H.A.M., Zucolotto, V., 2019. Biosens. Bioelectron. 131, 149-155.
526 Ganganboina, A.B., Chowdhury, A.D., Doong, R. A., 2017a. Electrochim. Acta 245, 912-923.
527 Ganganboina, A.B., Doong, R. A., 2018. Sens. Actuators, B 273, 1179-1186.
528 Ganganboina, A.B., Doong, R. A., 2018b. Microchim. Acta 185, 526.
529 Ganganboina, A.B., Doong, R. A., 2019. Sci. Rep. 9(1), 7214.
530 Ganganboina, A.B., Doong, R. A., 2020. Environ. Sci.: Nano, 7, 228-237.
531 Ganganboina, A.B., Dutta Chowdhury, A., Doong, R. A., 2017b. ACS Appl. Mater.
532 Interfaces 10(1), 614-624.
533 Gao, Y., Zhou, Y., Chandrawati, R., 2020. ACS Appl. Nano Mater.. 3, 1, 1-21
534 Hall, A.J., Glass, R.I., Parashar, U.D., 2016. Taylor & Francis. 15(8), 949–951
535 Han, Z., Chen, L., Weng, Q., Zhou, Y., Wang, L., Li, C., Chen, J., 2018. Sens. Actuators, B
536 258, 508-516.
537 Holme, M.N., Rana, S., Barriga, H.M., Kauscher, U., Brooks, N.J., Stevens, M.M., 2018.
538 ACS Nano 12(8), 8197-8207.
539 Hong, S.A., Kwon, J., Kim, D., Yang, S., 2015. Biosens. Bioelectron. 64, 338-344.
540 Hwang, H.J., Ryu, M.Y., Park, C.Y., Ahn, J., Park, H.G., Choi, C., Ha, S.-D., Park, T.J., Park,
541 J.P., 2017. Biosens. Bioelectron.87, 164-170.

Khoris, I.M., Takemura, K., Lee, J., Hara, T., Abe, F., Suzuki, T., Park, E.Y., 2019. Biosens. Bioelectron. 126, 425-432.

Ku, A., Chan, C., Scollard, D., Reilly, R., 2017. J. Nucl. Med. 58, 673-673.

Maurya, V.K., Kumar, S., Saxena, S.K., Conventional Treatments of Water-Associated Infectious Diseases. 2020. Water-Associated Infectious Diseases, 105-118.

Nasrin, F., Chowdhury, A.D., Takemura, K., Lee, J., Adegoke, O., Deo, V.K., Abe, F., Suzuki, T., Park, E.Y., 2018. Biosens. Bioelectron.122, 16-24.

Oh, S., Kim, J., Tran, V.T., Lee, D.K., Ahmed, S.R., Hong, J.C., Lee, J., Park, E.Y., Lee, J., 2018. ACS Appl. Mater. Interfaces 10(15), 12534-12543.

Pan, J., Li, M., Luo, Y., Wu, H., Zhong, L., Wang, Q., Li, G., 2015. Appl. Surf. Sci. 333, 34-38.

Peng, X., Luo, G., Wu, Z., Wen, W., Zhang, X., Wang, S., 2019. ACS Appl. Mater. Interfaces 11(44), 41148-41156.

Sharmin, S., Islam, M.Z., Karal, M.A.S., Alam Shibly, S.U., Dohra, H., Yamazaki, M., 2016. Biochemistry 55(30), 4154-4165.

Takemura, K., Adegoke, O., Takahashi, N., Kato, T., Li, T.-C., Kitamoto, N., Tanaka, T., Suzuki, T., Park, E.Y., 2017. Biosens. Bioelectron. 89, 998-1005.

Vernekar, A.A., Sinha, D., Srivastava, S., Paramasivam, P.U., D'Silva, P., Mugesh, G., 2014. Nat. Commun. 5, 5301.

Weerathunge, P., Ramanathan, R., Torok, V.A., Hodgson, K., Xu, Y., Goodacre, R., Behera, B.K., Bansal, V., 2019. Anal. Chem. 91(5), 3270-3276.

Wu, Z., Guo, W.-J., Bai, Y.-Y., Zhang, L., Hu, J., Pang, D.-W., Zhang, Z.-L., 2018. Anal. Chem. 90(3), 1683-1690.

Xiong, L.-H., He, X., Zhao, Z., Kwok, R.T., Xiong, Y., Gao, P.F., Yang, F., Huang, Y., Sung, H.H.-Y., Williams, I.D., 2018. ACS Nano 12(9), 9549-9557.

567 Ye, H., Yang, K., Tao, J., Liu, Y., Zhang, Q., Habibi, S., Nie, Z., Xia, X., 2017. ACS Nano
568 11(2), 2052-2059.
569 Zang, F., Su, Z., Zhou, L., Konduru, K., Kaplan, G., Chou, S.Y., 2019. Adv. Mater., 1902331.

570

Supplementary data

Dual-modality sensor using liposome-based signal amplification technique for ultrasensitive norovirus detection

Akhilesh Babu Ganganboina,[1] Ankan Dutta Chowdhury[1], Indra Memdi Khoris[2], Fahmida Nasrin[2], Kenshin Takemura[2], Toshimi Hara[3], Fuyuki Abe[3], Tetsuro Suzuki[4], Enoch Y. Park[1,2,*]

[1] Research Institute of Green Science and Technology, Shizuoka University, 836 Ohya Suruga-ku, Shizuoka 422-8529, Japan

[2] Department of Bioscience, Graduate School of Science and Technology, Shizuoka University, 836 Ohya Suruga-ku, Shizuoka 422-8529, Japan

[3] Department of Microbiology, Shizuoka Institute of Environment and Hygiene, 4-27-2, Kita-ando, Aoi-ku, Shizuoka 420-8637, Japan

[4] Department of Infectious Diseases, Hamamatsu University School of Medicine, 1-20-1 Higashi-ku, Handa-yama, Hamamatsu 431-3192, Japan

E-mail addresses:
akhilesh.babu.ganganboina@shizuoka.ac.jp (ABG)
ankan.dutta.chowdhury@shizuoka.ac.jp (ADC)
Indra.memdi.khoris.17@shizuoka.ac.jp (IMK)
fahmida.nasrin.17@shizuoka.ac.jp (FN)
takemura.kenshin.16@shizuoka.ac.jp (KT)
toshimi1_hara@pref.shizuoka.lg.jp (TH)
fuyuki1_abe@pref.shizuoka.lg.jp (FA)
tesuzuki@hama-med.ac.jp (TS)
park.enoch@shizuoka.ac.jp (EYP)

---

[1] Corresponding author at: Research Institute of Green Science and Technology, Shizuoka University, 836 Ohya, Suruga-ku, Shizuoka 422-8529, Japan.
E-mail address: park.enoch@shizuoka.ac.jp (E.Y. Park). Tel (Fax): +81-54-238-4887)

Table S1. Kinetic parameters of V_2O_5 NPs.

Substrate	Km (mM)	V_{max} (10^{-7} M.min^{-1})
TMB	0.02	19.7
H_2O_2	0.04	20.9

Table S2. Comparison of the dual-modality VONP-LPs/MNP biosensor with recently reported methods in respect to linear range and detection limit.

Sensing matrix	Sample type	Linear range	Analytics time (mins)	LOD	Ref
Electrochemical					
AuNP-Peptide	Capsid protein and Clinical NoV	10^1–10^7 copies mL^{-1}	~ 60	7.8 copies mL^{-1}	Hwang et. al. (2017)
Graphene-AuNP	NoV-LP, NoV	100 pM to 3.5nM	~ 30	100 pM	Chand et. al. (2017)
Con A@Au electrode	Clinical NoV	10^2 and 10^6 copies mL^{-1}	-	35 copies mL^{-1}	Hong et. al. (2015)
Peptide-Au electrode	Clinical NoV	0 to 10^5 copies mL^{-1}	30	2.47 copies mL^{-1}	Beak et. al. (2019)
Optical					
AuNR@CdSeTe	Virus RNA	2–18 copies mL^{-1}	-	1.2 copies mL^{-1}	Han et. al. (2018)
Ag shell on Au NPs	NoV-LP and Clinical NoV	102–106 copies mL^{-1}	~ 60	13.2 copies mL^{-1}	Khoris et. al. (2019)
HRPzyme	Virus RNA	10–10^4 copies mL^{-1}	~ 50	1 copies mL^{-1}	Batule et. al. (2016)
AuNP-CdSeTeS QDs	NoV-LP and Clinical NoV	10^2–10^5 copies mL^{-1}	~ 10	95.0 copies mL^{-1}	Nasrin et. al. (2018)
VONP-LPs	NoV-LP and Clinical NoV	10 fg mL^{-1} 100 ng mL^{-1}	~ 20	4.1 fg mL^{-1}	This work
VONP-LPs	NoV-LP and Clinical NoV	10^2–10^7 copies mL^{-1}	~ 20	72 copies mL^{-1}	This work

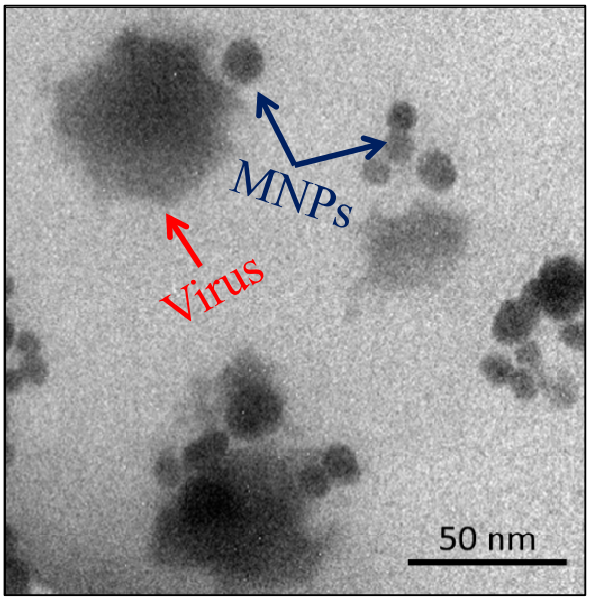

Fig. S1. TEM image of VONP-LPs@Nov-LPs/MNPs where the NoV-LPs are stained with Urinyl acetate.

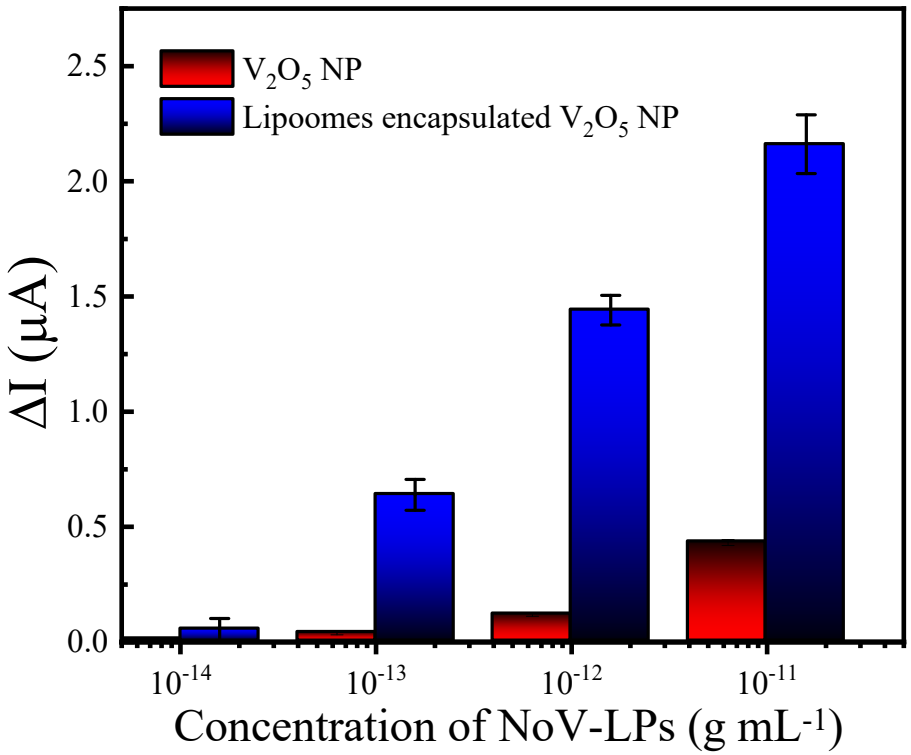

Fig. S2. Comparison of change in current using individual V_2O_5 NPs and liposome encapsulated V_2O_5 NPs functionalized with NoV antibody for detection of NoV-LPs.

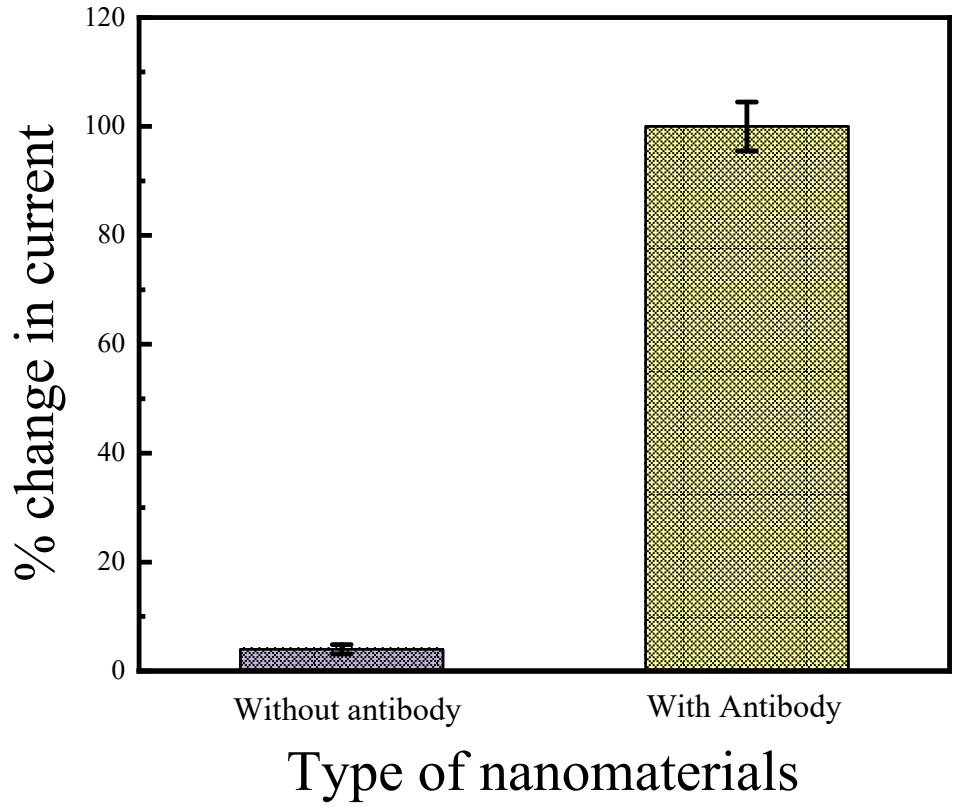

Fig. S3. The change of current intensity in response to nanomaterials with and without antibody conjugation.

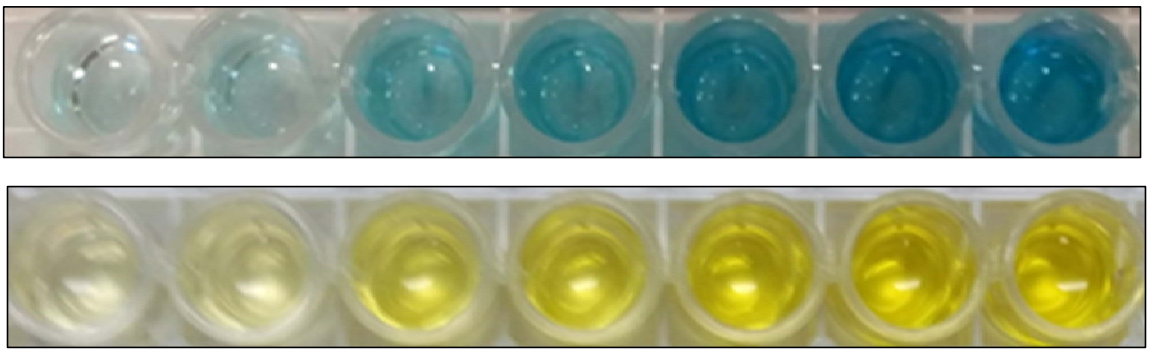

Fig. S4. Images of the change in color of TMB solution in the presence of various concentrations of NoV. The color intensity increases with the increase in NoV concentration and the color changes to yellow immediately on addition of 10% H_2SO_4.

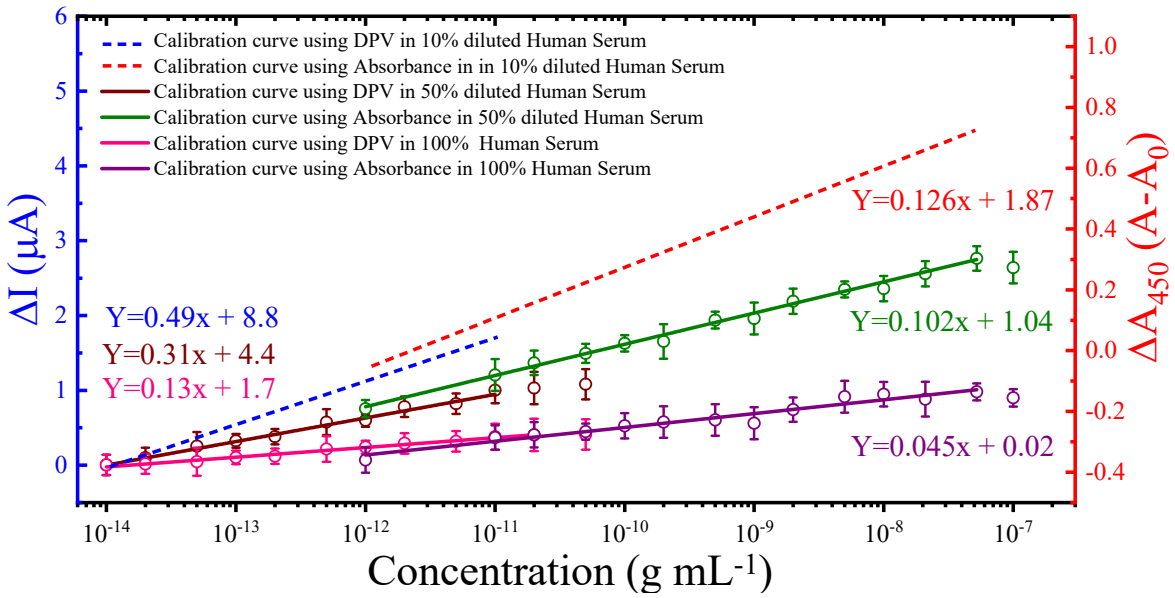

Fig. S5 Calibration curve for NoV-LPs using in 10%, 50% diluted and 100% human serum as sensing medium and its corresponding calibration line.

1. Materials and methods

1.1 Chemicals

Vanadium pentoxide (V_2O_5), Polyethylene glycol 600 (PEG), (3-aminopropyl)-triethoxysilane (APTES), N-(3-dimethylaminopropyl)-N-ethylcarbodiimide hydrochloride (EDC), N-hydroxysuccinimide (NHS) and dry toluene were purchased from Sigma-Aldrich (St Louis, USA). Sodium citrate, $FeCl_3 \cdot 6H_2O$ and $FeSO_4 \cdot 7H_2O$ were obtained from Wako Pure Chemical Industries Ltd (Osaka, Japan). 1,2-dioleoyl-sn-glycero-3-phospho-(1'-rac-glycerol) (DOPG), 1,2-distearoyl-sn-glycero-3-phosphoethanolamine-N-[amino(polyethylene glycol)-2000] (DSPE), and 1-palmitoyl-2-oleoyl-sn-glycero-3-phosphocholine (DOPC) were obtained from Avanti polar lipids (Alabaster, AL, USA). 28% (w/v) ammonia solution is purchased from Duksan Pure Chemical Co., Ltd. (Ansan-si, South Korea). Succinimidyl 4-(N-maleimidomethyl) cyclohexane-1-carboxylate (SMCC) was procured from Thermo Fisher Scientific K.K. (Tokyo Japan). All aqueous solutions were prepared by using high-purity bidistilled deionized water (> 18.2 MΩ cm) unless otherwise mentioned.

1.2 Preparation of V_2O_5 nanoparticles (V_2O_5 NPs)

To synthesize V_2O_5 NPs, 1 mmol bulk V_2O_5 powder was mixed with 22.5 ml distilled water followed by addition of 2.5 ml 30% H_2O_2 and stirred vigorously for 2 h.(Pan et al., 2015) 500 mg polyethylene glycol 600 (PEG-600) was dissolved in the above transparent orange solution, transferred to Teflon lined stainless steel autoclave, and maintained at 200°C for 6 h. Thus formed product was washed with ethanol and distilled water for three times and dried at 60°C for 12 h. The dried powder was annealed at 350°C for 30 min in air and stored for further use.

1.3 Preparation of APTES coated MNPs

In brief, 1.165 g of $FeCl_3 \cdot 6H_2O$ and 0.6 g of $FeSO_4 \cdot 7H_2O$ were dispersed in 200 mL deionized and heated to 60°C under the nitrogen atmosphere with vigorous stirring. To precipitate the surface-immobilized Fe^{2+} and Fe^{3+} ions, 8 M NH_4OH solution (20 mL) was slowly added. pH of reaction mixture was maintained at about 11, to ensure the complete conversion of iron ions to iron oxides. The resulting black precipitate was aged at 70°C for 6 h, and then washed with water and magnetic separation. The obtained MNPs were dried at 70°C for 12 h. As synthesized MNPs were coated with APTES by using the standard method of silanization.(Ganganboina et al., 2017a) Dry toluene was used as reaction medium to dissolve APTES and then the above prepared MNPs were added to it in inert atmosphere. The mixture was refluxed at 120°C for 20 h under continuous stirring to obtain APTES-coated MNPs. Finally, the solid phase was separated by filtration, rinsed with fresh toluene to remove the unreacted APTES, dried overnight at 60°C and stored for further usage.

1.4 Preparation of V_2O_5 NPs-encapsulated liposome (VONP-LPs)

Briefly, 200 µL of 10 mM phospholipid mixtures solution containing DOPC:DOPG:DSPE (50:40:10) in chloroform are added into 5 mL round bottom glass vials.(Sharmin et al., 2016) Solvent was vaporized by flowing 99.9% nitrogen gas to produce a thin homogeneous lipid film along the glass wall. The solvent was completely vaporized by placing the bottle containing the dry lipid film in a vacuum desiccator connected to a rotary vacuum pump for more than 12 h and then stored at − 20°C. Twenty µL of water was added into this glass vial, and the mixture was incubated at 45°C for 10 min (prehydration). For hydration, V_2O_5 NPs solutions of 50, 100, 150 and 200 µg mL^{-1} were prepared in HEPES. The dry lipid films stored at −20°C are hydrated with above prepared V_2O_5 NPs solutions for

30 min and agitated on a vortex shaker to make sure the lipid film has completely separated from the walls of glass vials forming lipid suspension. The monodispersed 200 nm VONP-LPs, were obtained extruding the lipid suspension for 3 times through a 200 nm pore sized polycarbonate membrane (Merck, Carrigtwohill, Ireland) using a micro injection.

1.5 Characterizations

Transmission electron microscopy (TEM) images were obtained using a TEM (JEM-2100F; JEOL, Ltd., Tokyo, Japan) operated at 100 kV to check the size and surface morphology of prepared nanomaterials. Dynamic light scattering (DLS) measurements were carried out using a Zetasizer Nano series (Malvern Inst. Ltd., Malvern, UK). X-ray diffraction (XRD) patterns were recorded using Bruker D8 X-ray diffractometer with Ni-filtered Cu Kα radiation (λ = 1.5406 Å) and X-ray photoelectron spectroscopy (XPS) was performed with an ESCA Ulvac-PHI 1600 photoelectron spectrometer from physical electronics using Al Kα radiation photon energy at 1486.6 ± 0.2 eV. UV–Vis absorption spectra measurements were carried out using a filter-based multimode microplate reader (Infinite F500; TECAN, Ltd, Männedorf, Switzerland). Cyclic voltammetry and electrochemical DPV was performed on SP-150 (BioLogic.inc, Tokyo, Japan) using conventional three-electrode cell containing Au electrode (4 mm in diameter), saturated Ag/AgCl and platinum wire as the working, reference and counter electrodes, respectively (EC frontier, Tokyo, Japan).

1.6 Peroxidase-like catalytic activity of V_2O_5 NPs

The peroxidase-like activity of the V_2O_5 NPs was evaluated from the catalytic oxidation of TMB by H_2O_2. A typical concentration-dependent experiment was performed at room temperature with dilution series of V_2O_5 NPs in the working solution, containing 40

mM TMB solution and 500 mM H_2O_2 (1:9 v/v) in deionized water. To determine the kinetic of the catalytic oxidation of TMB with V_2O_5 NPs as the nanozyme, steady-state kinetic assay was carried out by reacting 100 µL V_2O_5 (25 nM), 50 µL TMB (0.05 mM – 1.2 mM) and 450 µL H_2O_2 (0.01 mM – 0.5 mM) at 653 nm using UV−vis spectroscopy. The initial reaction data on the absorbance vs time was analyzed to measure the initial velocity of each concentration. The initial velocity was visualized by Michelin-Menten plot and Lineweaver-Burk reciprocal plot to determine the kinetic parameter, k_m and v_{max}.

1.7. Preparation of Anti-NoV antibody-conjugated VONP-LPs and MNPs

Anti-NoV antibody which is widely reactive to genogroup II (Monoclonal antibody NS14) was utilized. NS14 (isotype - IgG) was acquired from spleen cells of mice immunized orally. Thus obtained antibody was purified by protein G and the concentration is 0.3 mg mL^{-1}. Initially, the VONP-LPs are conjugated with 6 mg of sulfo-SMCC and the Anti-NoV antibody was conjugated with iminothiolane by incubation for 60 min at room temperature.(Ku et al., 2017) Then SMCC-conjugated VONP-LPs and iminothiolane-conjugated antibody solutions were mixed and incubated for 1 h at room temperature. The amine group of DSPE in VONP-LPs conjugates with the carboxylic group of antibody. The conjugate mixture was continuously stirred overnight and unbound antibodies were separated by centrifugation and further dissolved in 2 mL of deionized water. In addition, Anti-NoV antibody was conjugated with the functional amine group of APTES on MNPs surface by the standard EDC/NHS protocol.

1.8. Preparation of NoV-LPs and clinically isolated NoV

NoV-like particles (NoV-LPs) were expressed in *Trichoplusia ni*, BTL-Tn 5B1-4 (Tn5) by transfection of recombinant baculovirus TCN-VP1 (Invitrogen, San Diego, CA, USA). Thus expressed NoV-LPs was purified and then quantified in accordance to the standard method for virus like particle preparation.(Ahmed et al., 2017)

NoV was obtained from clinical feces samples collected from infected patients with infectious gastroenteritis, including foodborne illness, as determined by inspections based on laws and ordinances. One hundred μg of fecal sample was added to 900 μL of phosphate-buffered saline (PBS, pH 7.4), solids were separated and the supernatant was used for the detection sample. The NoV concentration of these supernatants was evaluated to be GⅡ.2: 6.2×10^7 RNA copy mL^{-1}, GⅡ.3: 7.2×10^8 RNA copy mL^{-1}, and GⅡ.4: 5.7×10^7 RNA copy mL^{-1}, respectively, by Real-time-PCR. Therefore, the detection performance was evaluated in ranging from 10^2 to 10^7 RNA copy mL^{-1} NoV in feces sample. This NoV sampling was performed according to the guideline, after obtaining appropriate approvals from Ethics Committee of Environment and Hygiene Institute in Shizuoka Prefecture (September 14, 2016).

1.9. Quantification of clinically isolated NoVs using real-time PCR

NoV RNAs were extracted from 10% fecal suspension in PBS by using QIAamp Viral RNA Mini Kit (QIAGEN, Tokyo Japan), and after treated with recombinant DNase (RNase-free) (TaKaRa Bio Inc., Shiga, Japan), reverse transcription was performed by using Prime Script RT Reagent Kit (Perfect Real Time) (TaKaRa Bio Inc.). Obtained cDNAs were detected and quantified by real-time PCR technique by using Premix EX Taq (Probe qPCR) (TaKaRa Bio Inc.) in accordance with the notice of the Ministry of Health, Labor and Welfare, Japan (2003).

1.10. Detection of NoV-LPs and Norovirus.

Anti-NoV antibody-VONP-LPs and MNPs were mixed with different concentration of the NoV-LPs and also clinically isolated NoVs and further incubated for 10 min. Then an external magnet was placed at the bottom of the mixture to separate the VONP-LPs/NoV-LP/MNP sandwich structure. After the separation, the mixture was re-dispersed with fresh buffer in microplate reader and 5 μL of 0.1 mM Triton solution was added to disrupt the liposome and release the encapsulated V_2O_5 NPs. One hundred μL of prepared substrate solution (4 M H_2O_2 and 40 mM TMB solution in 0.4 M HOAc/NaOAc buffer, pH 4.0) was added to the wells and blue color developed rapidly. In addition to stop the reaction, 10% H_2SO_4 was added after 5 min, resulting in changing blue color to yellow. Finally, the absorbance was recorded using a microplate reader (Model 680, Bio-Rad, Hercules, CA). For the electrochemical determination, the same reaction as mentioned above was carried out in a separate tube and the released V_2O_5 NPs from captured liposomes was deposited on graphene modified electrodes and DPV was used to record the electrochemical output signal of V_2O_5 NPs for the ultrasensitive detection of NoV-LPs. 0.1 M H_2SO_4 was used as electrolyte. This VONP-LPs/NoV-LP/MNP based NoV sensor was optimized and improved using NoV-LPs and implemented to detect NoV according to the optimized protocol. For the specificity of the developed dual-modality sensor, six control experiments were performed: the four control experiments 100 pg mL^{-1} of HEV-LP, 10^4 copies mL^{-1} of WSSV, 10^3 PFU mL^{-1} of Zika virus and 20 μg mL^{-1} of Influenza and another two control experiment using BSA and 10 times diluted human serum, without any virus as reagent blank was also performed using the same procedure as the NoV sample.

References

Ahmed, S.R., Takemeura, K., Li, T.-C., Kitamoto, N., Tanaka, T., Suzuki, T., Park, E.Y., 2017. Biosens. Bioelectron. 87, 558-565.

Ganganboina, A.B., Chowdhury, A.D., Doong, R. A., 2017. Electrochim. Acta 245, 912-923.

Ku, A., Chan, C., Scollard, D., Reilly, R., 2017. J. Nucl. Med. 58, 673-673.

Pan, J., Li, M., Luo, Y., Wu, H., Zhong, L., Wang, Q., Li, G., 2015. Appl. Surf. Sci. 333, 34-38.

Sharmin, S., Islam, M.Z., Karal, M.A.S., Alam Shibly, S.U., Dohra, H., Yamazaki, M., 2016. Biochemistry 55(30), 4154-4165.